Photon–Photon and Electron–Photon Colliders with Energies Below a TeV

Mayda M. Velasco* and Michael Schmitt
Northwestern University, Evanston, Illinois 60201, USA
Gabriela Barenboim and Heather E. Logan
Fermilab, PO Box 500, Batavia, IL 60510-0500, USA
David Atwood
Dept. of Physics and Astronomy, Iowa State University, Ames, Iowa 50011, USA
Stephen Godfrey and Pat Kalyniak
Ottawa-Carleton Institute for Physics Department of Physics, Carleton University, Ottawa, Canada K1S 5B6
Michael A. Doncheski
Department of Physics, Pennsylvania State University, Mont Alto, PA 17237 USA
Helmut Burkhardt, Albert de Roeck, John Ellis, Daniel Schulte, and Frank Zimmermann
CERN, CH-1211 Geneva 23, Switzerland
John F. Gunion
Davis Institute for High Energy Physics, University of California, Davis, CA 95616, USA
David M. Asner, Jeff B. Gronberg,† Tony S. Hill, and Karl Van Bibber
Lawrence Livermore National Laboratory, Livermore, CA 94550, USA
JoAnne L. Hewett, Frank J. Petriello, and Thomas Rizzo
Stanford Linear Accelerator Center, Stanford University, Stanford, California 94309 USA

We investigate the potential for detecting and studying Higgs bosons in $\gamma\gamma$ and $e\gamma$ collisions at future linear colliders with energies below a TeV. Our study incorporates realistic $\gamma\gamma$ spectra based on available laser technology, and NLC and CLIC acceleration techniques. Results include detector simulations. We study the cases of: a) a SM-like Higgs boson based on a devoted low energy machine with $\sqrt{s_{ee}} \leq 200$ GeV; b) the heavy MSSM Higgs bosons; and c) charged Higgs bosons in $e\gamma$ collisions.

1. Introduction

The option of pursuing frontier physics with real photon beams is often overlooked, despite many interesting and informative studies [1]. The high energy physics community has focussed on charged particle beams for historical reasons, and risks missing an excellent opportunity to do exciting physics in the near future, if the $\gamma\gamma$ option is ignored. In the context of the next generation of accelerators, most people are comfortable with the idea of colliding TeV electrons and positrons, but have not really considered the idea of colliding 100 GeV photons. Yet this is now feasible, and could deliver crucial and unique information on the Higgs sector. For example, $\gamma\gamma$ collisions offer a unique capability to measure the two-photon width of the Higgs and to determine its CP composition through control of the photon polarization. Also, $\gamma\gamma$ collisions offer one of the best means for producing a heavy Higgs boson singly, implying significantly greater mass reach than e^+e^- production of a pair of Higgs bosons. Our Snowmass working group [2] presents a realistic assessment of the prospects for these studies based on the current NLC machine and detector designs [3, 4] for $\sqrt{s_{ee}}$ up to around 600 GeV, and CLIC-1 [5, 6] with $\sqrt{s_{ee}} \simeq 150$ GeV. The expectations for TESLA [7, 8] can be deduced by multiplying the NLC yields by a factor of 1.5 to 2, due the larger repetition rate and bunch charge.

*Coordinator: mayda.velasco@cern.ch
†Coordinator: gronberg1@llnl.gov

2. The machine

There is great interest in an e^+e^- linear collider, and one is likely to be built somewhere in the world. Here we consider 75 GeV electrons for NLC and CLIC-1, and 100 to 350 GeV for NLC. At and above these energies, all types of machines: NLC/JLC, TESLA and CLIC, have suitable luminosities for a $\gamma\gamma$ collider. In all cases, we assume e^+e^- collisions as our starting point, and the electrons to be 80% longitudinally polarized. We prefer to only use electrons, because one can obtain higher luminosity and total $\gamma\gamma$ polarization than with positrons.

In all cases, a $\gamma\gamma$ interaction region would fit into the present plans. Both NLC [3] and TESLA [8] have plans for a second, lower energy, interaction region that can be used for $\gamma\gamma$ collisions, while the CLIC-1 based design that we have developed assumes only one dedicated $\gamma\gamma$ interaction region. We refer to the CLIC-1 based design as CLICHE [6], the "CLIC Higgs Experiment."

The photon beams required in a $\gamma\gamma$ collider would be produced via the Compton backscattering of laser light off the high-energy electron beam. In the electron–laser collision at the conversion point, the maximum energy of the scattered photons is

$$\omega_m = \frac{x}{x+1}E_0; \quad x \approx \frac{4E_0\omega_0}{m^2c^4} \simeq 15.3\,[E_0/\mathrm{TeV}]\,[\omega_0/eV]\,,$$

where E_0 is the electron beam energy and ω_0 the energy of the laser photon. In connection with NLC studies [3], the case has been considered of $E_0 = 250\,\mathrm{GeV}$, $\omega_0 = 1.17\,\mathrm{eV}$, i.e., a wavelength of 1.054μm, with a high power Mercury laser from the LLNL group. This would correspond to $x = 4.5$ and $\omega_m = 0.82E_0$.

The computation of the luminosity function $F(\gamma) = d\mathcal{L}_{\gamma\gamma}/d\gamma/\mathcal{L}_{\gamma\gamma}$ [9, 10], assuming a short (1–5 mm) distance from the electron–laser collision to the $\gamma\gamma$ interaction point, is shown in Figure 1 as a function of $\gamma = E_{\gamma\gamma}\sqrt{s_{ee}^{-1}}$ along with the $\langle\lambda\lambda'\rangle$ values, where the λ's are the resulting photon beam helicities. There are three independent choices for λ_e, λ'_e, P and P', where $\lambda_e = \frac{1}{2}P_e$ is the electron helicity and P is the laser polarization. In Figure 1 we give the results for three independent choices of relative electron and laser polarization orientations for the values of x relevant in our studies, $x = 5.69$, $x = 4.334$ and $x = 1.86$.

We observe that choice (I) of $\lambda_e = \lambda'_e = 0.4$, $P = P' = 1$ gives a large $\langle\lambda\lambda'\rangle$ and $F(\gamma) > 1$ for small to moderate γ. Therefore, it could be interesting with high energy machines seaching in a broad energy range for $J = 0$ particles like heavy Higgs bosons. In a machine with 315 GeV electrons and 1.054 μm lasers, for example, $x = 5.69$. It has been argued in the past that $x > 4.8$ is undesirable because it leads to pair creation. However, our studies, which include these effects, indicate that the resulting backgrounds are not a problem.

The choice (II) of $\lambda_e = \lambda'_e = 0.4$, $P = P' = -1$ yields a peaked spectrum with $\langle\lambda\lambda'\rangle > 0.85$ at the maximum. If we use 1.054 μm lasers, then a value of $x = 1.86$ for 103 GeV electrons is obtained, and we can see that the $\gamma\gamma$ spectrum peaks at $E_{\gamma\gamma}^{\mathrm{peak}} \sim 120\mathrm{GeV}$. This would be an optimal setting for light Higgs boson studies. If a tripler is added to the laser system, then the wavelength is reduced by a factor of three, and a $\gamma\gamma$ spectrum peaking at $E_{\gamma\gamma}^{peak} = 120\mathrm{GeV}$ is obtained by operating at $\sqrt{s_{ee}} = 160\mathrm{GeV}$, yielding $x = 4.334$. The realistic spectra and luminosities for such cases are plotted in Figure 2, for CLICHE with $x = 4.334$ and NLC with $x = 1.86$. These results were produced with the CAIN [14] program, which takes into account the beamstrahlung, secondary collisions between scattered electrons and photons from the laser beam and other non-linear effects. The result is a substantial enhancement of the luminosity in the low-$E_{\gamma\gamma}$ region compared to the simple predictions given in Figure 1. The improvement for $x = 4.334$ as compared to $x = 1.86$ is clear. A summary of the expected luminosities at $E_{\gamma\gamma}^{\mathrm{peak}}$ running with this polarization configuration is shown in Table I, for different electron beam energies.

Finally, the choice (III) of $\lambda_e = \lambda'_e = 0.4$, $P = 1, P' = -1$ gives a broad spectrum, but never achieves large $\langle\lambda\lambda'\rangle$. Large values of $\langle\lambda\lambda'\rangle$ are important for suppressing the $c\bar{c}$ and $b\bar{b}$ continuum background to Higgs detection, whose leading tree-level term $\propto 1 - \langle\lambda\lambda'\rangle$, making this configuration not useful for Higgs studies.

3. Physics Opportunities—Higgs Factories

All the studies shown below use JETSET fragmentation, the event mixture predicted by PYTHIA (passed through JETSET) [11], and the LC Fast MC detector simulation within ROOT [12], which

Table I Luminosities for $J = 0$ component of the $\gamma\gamma$ energy spectra at $E_{\gamma\gamma}^{\rm peak}$ assuming $\lambda_e = \lambda'_e = 0.4$, $P = P' = -1$, choice (II). Values for different machines and beam energies tuned as a Higgs Factory, $M_{\rm Higgs} \simeq E_{\gamma\gamma}^{\rm peak}$, are given. $\langle\lambda\lambda'\rangle$ is given at the energy corresponding to $E_{\gamma\gamma}^{\rm peak}$.

E_e (GeV)	$\mathcal{L}_{\gamma\gamma}^{\rm peak}$ (fb^{-1}/{bin width GeV})	$E_{\gamma\gamma}^{\rm peak}$ (GeV)	$\langle\lambda\lambda'\rangle$	comment
CLIC–75	4.7 / 3.33	115.	0.94	22000 Higgs/year(10^7 sec) in SM
NLC –80	1.7 / 3.33	120.	0.87	11000 Higgs/year(10^7 sec) in SM
NLC –103	1.5 / 3.33	120.	0.85	9500 Higgs/year(10^7 sec) in SM
NLC –267.5	3.4 /11.13	406.	0.80	varies, *i.e.* see Fig. 10
NLC –315	3.4 /13.10	478.	0.79	varies, *i.e.* see Fig. 10

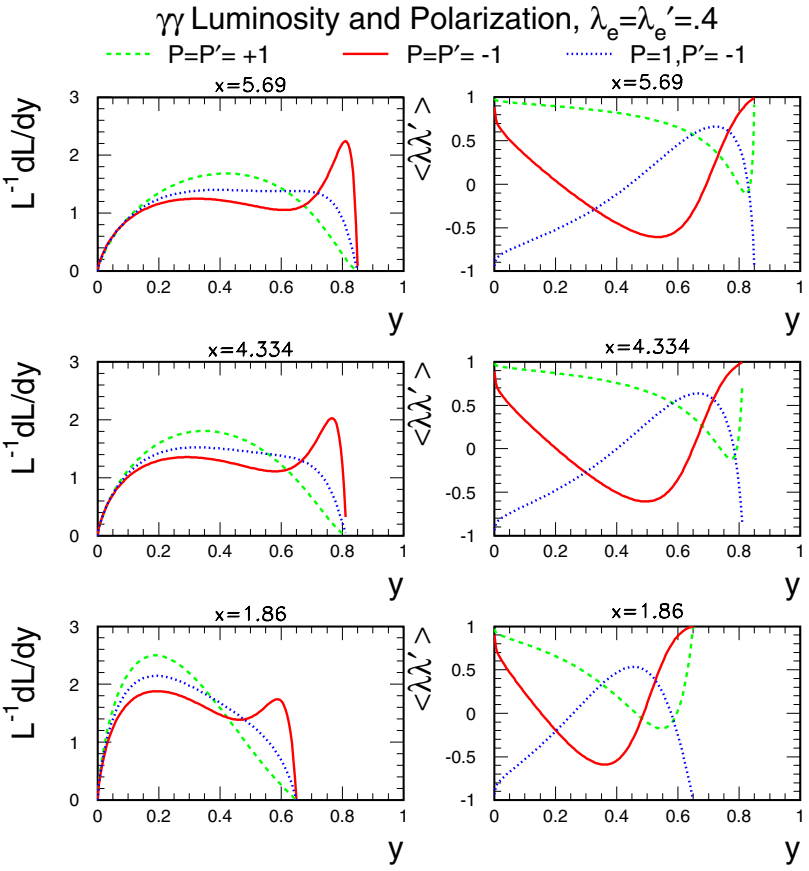

Figure 1: The normalized differential luminosity $1/(\mathcal{L}_{\gamma\gamma})(d\mathcal{L}_{\gamma\gamma})/(d\gamma)$ and the corresponding $\langle\lambda\lambda'\rangle$ for $\lambda_e = \lambda'_e = .4$ (80% polarization) and three different choices of the initial laser photon polarizations P and P'. The distributions shown are for $\rho^2 \ll 1$ [9, 10]. Results for $x = 5.69$, $x = 4.334$ and $x = 1.86$ are compared.

includes calorimeter smearing and the detector configuration. The signal is generated using PANDORA plus PYTHIA/JETSET [13]. The luminosity and polarization predictions from the CAIN [14] Monte Carlo were used to produce the beam spectra.

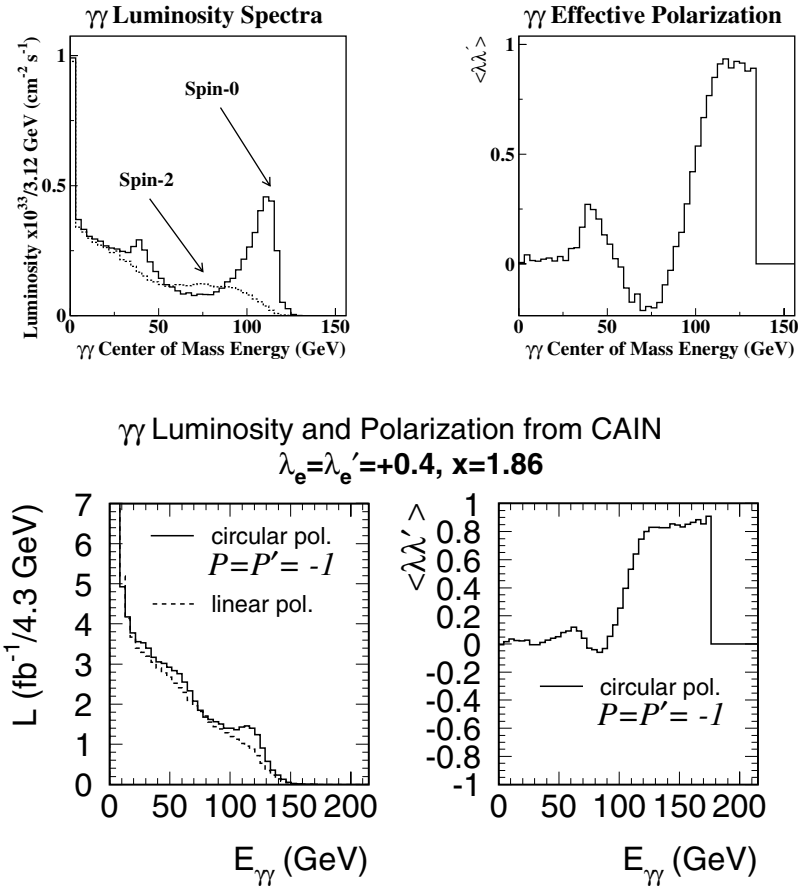

Figure 2: (a) Luminosity spectra and beam polarization as functions of $E_{\gamma\gamma}$ for the CLIC-1 parameters for 75 GeV electrons. (b) Luminosity spectra and beam polarization as functions of $E_{\gamma\gamma}$ for the NLC parameters for 103 GeV electrons. Also plotted is the corresponding value of $\langle\lambda\lambda'\rangle$ given by $\langle\lambda\lambda'\rangle = (L_{J_z=0} - L_{J_z=2})/(L_{J_z=0} + L_{J_z=2})$.

3.1. Light Higgs Measurements

a. Mass measurement:

The cross sections for a Higgs boson masses around 115 GeV as functions of $E_{CM}(e^-e^-)$ for unpolarized electrons are shown in Figure 3(a). We see that the cross section rises rapidly for $E_{CM}(e^-e^-)$ between 140 and 160 GeV. This feature, combined with the large value of $\mathcal{B}r(H \to b\bar{b})$, can be used to measure the Higgs mass by sweeping across the threshold for Higgs production and measuring how the number of $\bar{b}b$ events increases. Since the position of this threshold depends on the Higgs mass, a scan offers the possibility to measure the Higgs mass kinematically, as developed in [15].

We have studied this possibility in the context of $\gamma\gamma$ Higgs factories, constructed with NLC and CLIC based technologies, assuming that the Higgs mass is already known to within a GeV or so, from the Tevatron or the LHC. As shown in Figure 4, there is a point of optimum sensitivity to the Higgs mass a few GeV below the peak of the cross section. There is another point close to the maximum of the cross section, at which there is no sensitivity to the Higgs mass, and with maximum sensitivity to $\Gamma_{\gamma\gamma}$, allowing the separation of these two quantities. These points are illustrated in Figure 4. This translates into an error on the inferred Higgs mass of 100 MeV. More details for our analysis can be found in [6].

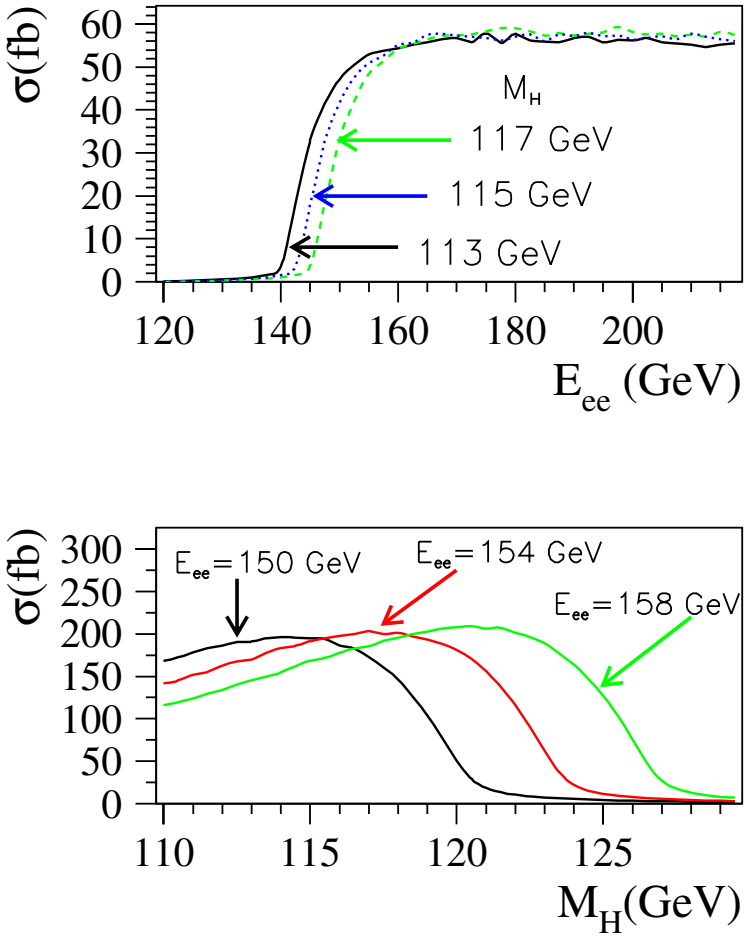

Figure 3: (a) The cross sections for $\gamma\gamma \to H$ for different values of m_H as functions of $E_{CM}(e^-e^-)$ for unpolarized photons. (b) The cross section for $\gamma\gamma \to H$ as a function of m_H for three different values of $E_{CM}(e^-e^-)$. Here the electrons are assumed to be 80% polarized longitudinally, and the lasers circularly polarized, so that the produced photons are highly circularly polarized at their peak energy.

b. $H \to \bar{b}b$*:*

Our analysis includes perturbative QCD backgrounds, including $\gamma\gamma \to \bar{b}b(g)$ and $\gamma\gamma \to \bar{c}c(g)$. The $\bar{q}q$ backgrounds are suppressed by choosing like polarizations for the colliding photons, but this suppression is not so strong when the final states contain additional gluons. We assume that there will be a 3.5% $c\bar{c}$ contamination and that the b tagging is 70% efficient for the double tag events. The final reconstruction efficiency is expected to be 30%. More details for our analysis can be found in [6, 18].

In the CLICHE design the mass resolution is around 6 GeV with a jet energy resolution of $\sigma_E = 0.6 \times \sqrt{E}$. The distribution in the di-jet invariant mass, m_{jets}, for a $m_H = 115$ GeV Higgs found in this study is shown in Figure 5. A clear signal peak can be seen above sharply falling backgrounds. Including the three bins nearest to $m_{jets} \sim 115$ GeV, we obtain 4704 signal events and 1046 background events. Thus, the signal-to-background ratio (S/B) is expected to be 4.5 after all cuts, and the statistical precision in the signal rate measurement is expected to be 2.3%. If the Higgs factory is made with a 103 GeV electrons instead of 75 GeV the S/B = 2.5 is not so favorable, because of the broader $\gamma\gamma$ energy distribution (see Table I and Fig. 2).

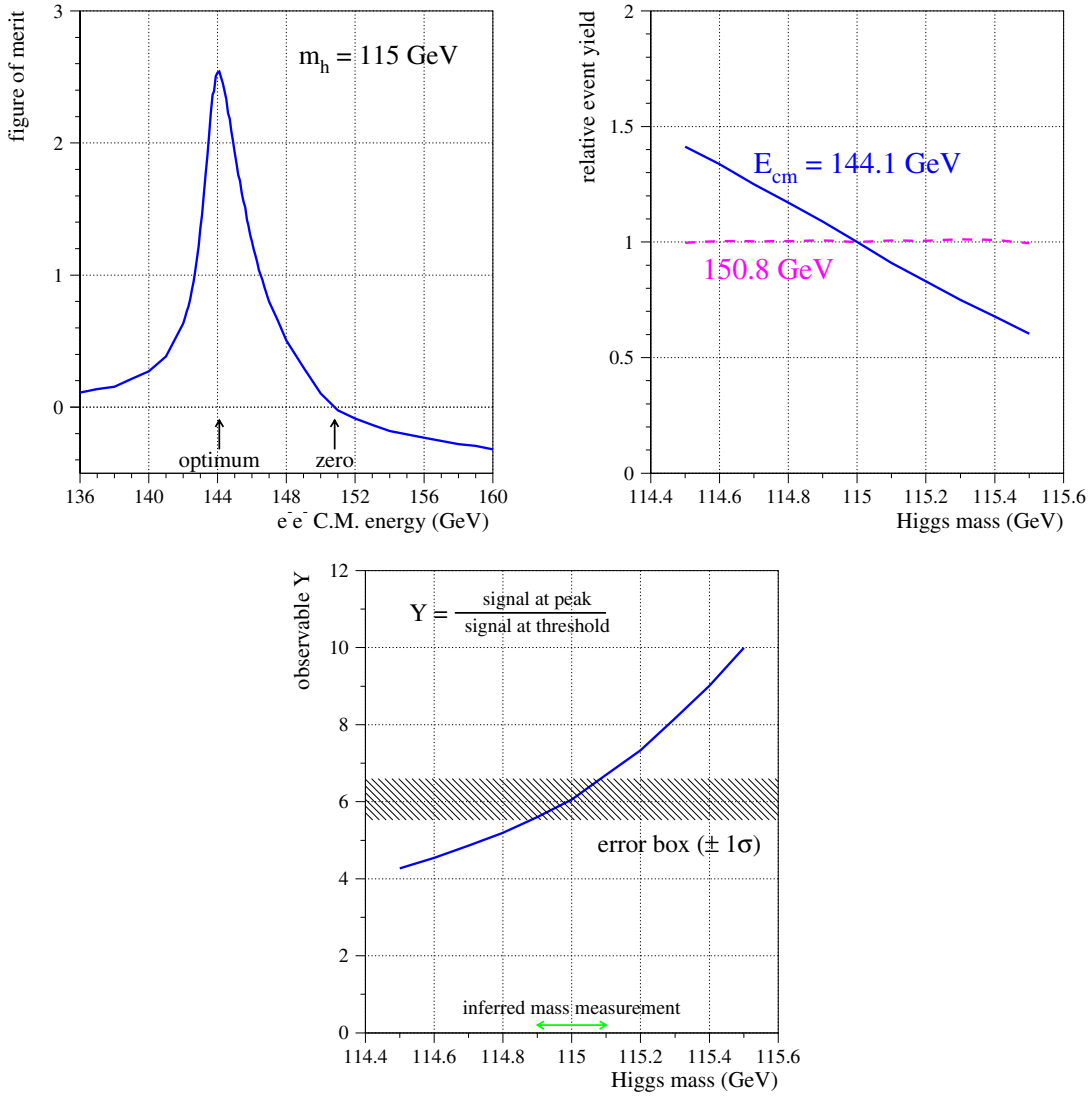

Figure 4: (a) A figure of merit quantifying the measurement error on the mass as a function of the e^-e^- center-of-mass energy. The optimum and zero sensitivity points are marked. (b) Relative yield for a 115 GeV Higgs boson at the point of optimum sensitivity and zero sensitivity to m_H. (c) Behavior of the observable $Y = (N_{\rm peak} - N_{\rm below} \cdot r_p)/(N_{\rm threshold} - N_{\rm below} \cdot r_t)$ as a function of m_H, and the projected error, where N is the number of events in a mass window logged at the peak, on the threshold, and below threshold, and r_p and r_t are scale factors to relate the background data taken below threshold to the expectation at peak and at threshold.

c. $H \to$ WW*:*

Observation of this decay mode is extremely difficult at high-energy $\gamma\gamma$ colliders, because of the large cross section for W pair production. If the $\gamma\gamma$ center-of-mass energy is below the W^+W^- threshold, however, the continuum production of W pairs is greatly reduced, allowing the observation of resonant production through a Higgs boson. The sharp peak in the $\gamma\gamma$ luminosity function seen in Figure 2 plays a key role here. Figure 6(a) compares the cross sections for the continuum W pair production with the Higgs resonance curve. As shown, the cross sections for $\sigma(\gamma\gamma \to W^+W^-)$ and $\mathcal{B}r(H \to W^+W^-) \times \sigma(\gamma\gamma \to H)$ are comparable, if $E_{CM}(e^-e^-) = 150$ GeV for a $m_H = 115$ GeV. One significant difference between the two type of events is the energy distribution of the W^+W^- pairs, as illustrated in Figure 6(b).

Our study is concentrated on the hadronic decays of the W pairs as described in [6]. After all cuts we have a 29% reconstruction efficiency. A comparison of the signal and the background

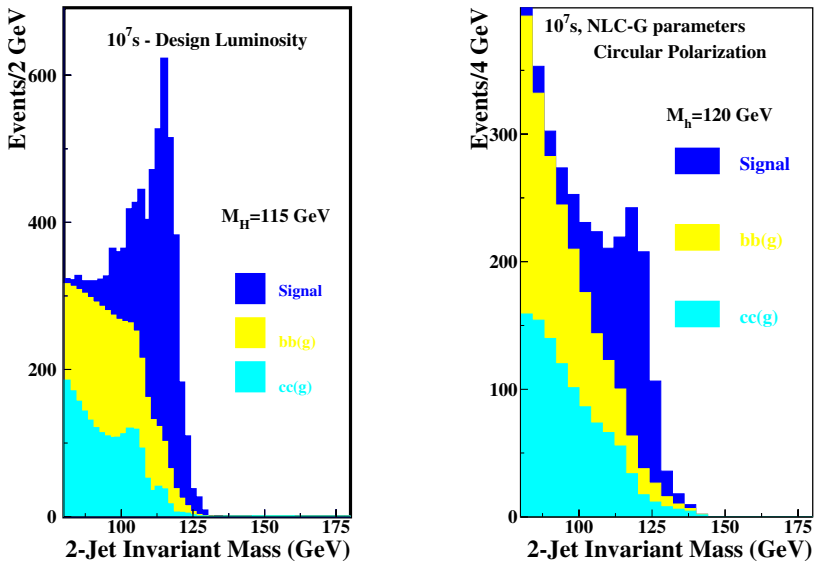

Figure 5: *Observability of the $H \to \bar{b}b$ decay mode at CLICHE with $\sqrt{s_{ee}} = 150$ GeV [6], and at NLC with $\sqrt{s_{ee}} = 206$ [3].*

after cuts is given in Figure 6(c), which corresponds to a signal-to-background ratio of 1.3, and the statistical precision in the signal rate measurement is expected to be 5%.

d. $H \to \gamma\gamma$:

The decay $H \to \gamma\gamma$ is very rare. However, the number of Higgs events is large at a $\gamma\gamma$ collider, so an interesting number of $H \to \gamma\gamma$ events would be produced. Furthermore, the backgrounds are expected to be quite small, below 2 fb [19], since there is no tree-level coupling of photons, and the box-mediated processes for $\gamma\gamma \to \gamma\gamma$ are peaked very sharply in the forward direction. Initial estimates indicate that a clear peak in the $\gamma\gamma$ mass distribution should be observable.

The number of events produced in this channel is proportional to $\Gamma^2_{\gamma\gamma}/\Gamma_{\rm total}$. The quadratic dependence is interesting, because if $\Gamma_{\rm total}$ could be measured elsewhere, a small error on $\Gamma_{\gamma\gamma}$ would be obtained. In Fig. 7, we can see that a 8% measurement of $\Gamma^2_{\gamma\gamma}/\Gamma_{\rm total}$ can be made with an integrated luminosity of 175 fb^{-1} or 40 fb^{-1} at the $\mathcal{L}^{\rm peak}_{\gamma\gamma}$ at CLICHE. From the comparison in Table I, we can see that this requires around one year of data taking at CLICHE, and almost two times longer for NLC.

3.2. Using Higgs factory measurements: the MSSM

e. $h \to b\bar{b}$ and $h \to$ WW:*

Taking the ratio of rates $(\gamma\gamma \to h \to b\bar{b})/(\gamma\gamma \to h \to {\rm WW}^*)$, the production cross section, total Higgs width and luminosity uncertainty cancel, yielding the ratio of Higgs partial widths $\Gamma(h \to b\bar{b})/\Gamma(h \to {\rm WW}^*)$ with about 6% statistical precision. In the MSSM, this ratio can deviate from its Standard Model (SM) value.

The SM ratio $\Gamma(H_{\rm SM} \to b\bar{b})/\Gamma(H_{\rm SM} \to {\rm WW}^*)$ depends strongly on the Higgs mass, varying by three orders of magnitude over the range $100\,{\rm GeV} < m_H < 160\,{\rm GeV}$. The Higgs mass measurement at the Photon Collider with an uncertainty of 100 MeV yields a 1% uncertainty in $\Gamma(H_{\rm SM} \to b\bar{b})/\Gamma(H_{\rm SM} \to {\rm WW}^*)$. This uncertainty is small compared to the expected experimental uncertainty. An additional theoretical uncertainty of 3.5% in $\Gamma(H_{\rm SM} \to b\bar{b})$ is due to the uncertainties in the b quark mass and in α_s [20].

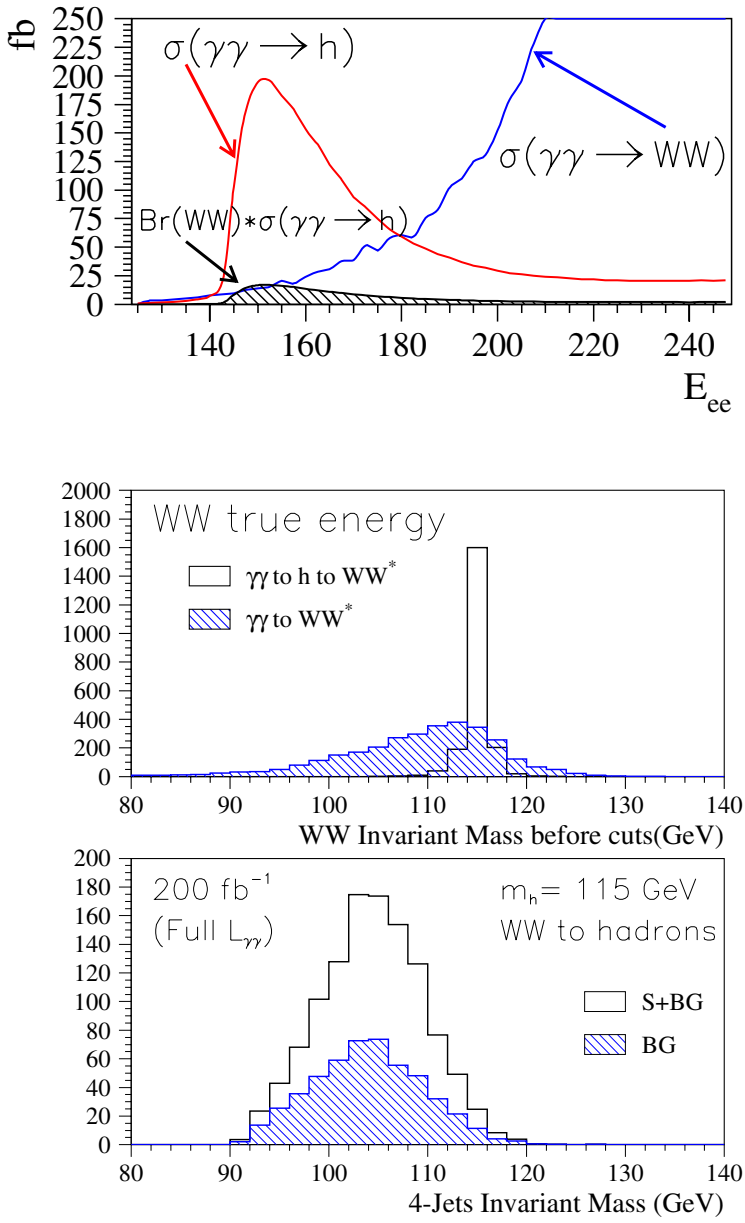

Figure 6: (a) Cross sections for $\gamma\gamma \to h$, $\gamma\gamma \to h \times \mathcal{B}r(h \to \mathrm{WW})$ for $m_H = 115$ GeV and $\gamma\gamma \to \mathrm{WW}$ production. (b) Comparison of the ideal invariant mass of the WW pairs from signal and background events. (c) Selection of the WW decay mode of the Higgs boson for $m_H = 115$ GeV, running at $\sqrt{s_{\gamma\gamma}} = 115$ GeV at CLICHE.

In the MSSM, $\Gamma(h \to b\bar{b})/\Gamma(h \to \mathrm{WW}^*)$ generally differs from its SM prediction, except in the decoupling limit [21]. For large pseudoscalar Higgs mass m_A and $\tan\beta$ greater than a few,

$$\frac{\Gamma(h \to b\bar{b})/\Gamma(H_{\mathrm{SM}} \to b\bar{b})}{\Gamma(h \to \mathrm{WW}^*)/\Gamma(H_{\mathrm{SM}} \to \mathrm{WW}^*)} \simeq 1 + \frac{4cm_Z^2}{m_A^2}\left[1 - \frac{\Delta_b}{1+\Delta_b}\right] + \mathcal{O}(m_Z^4/m_A^4), \qquad (1)$$

where c parameterizes the radiative corrections to the Higgs mixing angle α (see [20] for details) and Δ_b is a $\tan\beta$-enhanced SUSY correction to the relation between the b quark mass and its

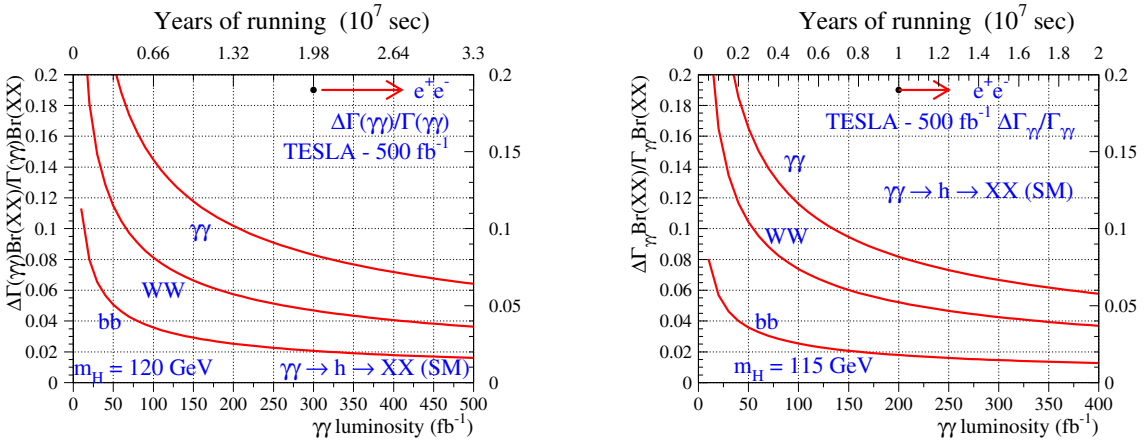

Figure 7: The expected precision in the $H \to \gamma\gamma$ decay width from direct measurements of $H \to \gamma\gamma$ for $m_H = 120$ GeV at NLC with 103 GeV electrons, and for $m_H = 115$ GeV at CLICHE with 75 GeV electrons. The precision is less than in the equivalent measurement of $H \to \mathrm{WW}, b\bar{b}$, but this observable is unique to a $\gamma\gamma$ collider.

Yukawa coupling [22, 23]. Figure 8(a) shows $\Gamma(h \to b\bar{b})/\Gamma(h \to \mathrm{WW}^*)$ in the MSSM normalized to its SM value as a function of m_A. For the chosen MSSM parameters, a 6% measurement of $\Gamma(h \to b\bar{b})/\Gamma(h \to \mathrm{WW}^*)$ will reveal a discrepancy from the SM at the 5σ (2σ) level for $m_A \lesssim 400\,\mathrm{GeV}$ (650 GeV).

The reach in m_A quoted above holds whenever the factor c in (1) is close to one, as it is over most of the MSSM parameter space. However, there are small parameter regions in which c is close to zero, leading to decoupling even at low values of m_A [20]. In such regions, $\Gamma(h \to b\bar{b})/\Gamma(h \to \mathrm{WW}^*)$ is very close to its SM value even for low m_A, and $\gamma\gamma$ collider measurements may not reveal a discrepancy from the SM.

f. $h \to b\bar{b}$ and $h \to \tau^+\tau^-$:

At the CERN Large Hadron Collider (LHC) the ratio $\Gamma(h \to \tau\tau)/\Gamma(h \to \mathrm{WW}^*)$ can be measured with a precision of about 15% using Higgs production in weak boson fusion [24]. Combining this measurement with $\Gamma(h \to b\bar{b})/\Gamma(h \to \mathrm{WW}^*)$ from the Photon Collider yields $\Gamma(h \to b\bar{b})/\Gamma(h \to \tau\tau)$ with a precision of about 16%. This ratio is particularly sensitive to Δ_b; at large $\tan\beta$ and large m_A,

$$\frac{\Gamma(h \to b\bar{b})/\Gamma(H_{\mathrm{SM}} \to b\bar{b})}{\Gamma(h \to \tau\tau)/\Gamma(H_{\mathrm{SM}} \to \tau\tau)} \simeq 1 - \frac{4cm_Z^2}{m_A^2}\frac{\Delta_b}{1+\Delta_b} + \mathcal{O}(m_Z^4/m_A^4). \tag{2}$$

Figure 8(b) shows $\Gamma(h \to b\bar{b})/\Gamma(h \to \tau\tau)$ in the MSSM normalized to its SM value as a function of m_A. The $\tan\beta$ dependence of Δ_b is clearly visible; at large $\tan\beta$ and $m_A \lesssim 225\,\mathrm{GeV}$, a 16% measurement of $\Gamma(h \to b\bar{b})/\Gamma(h \to \tau\tau)$ will reveal a discrepancy from the SM at the 2σ level for the chosen MSSM parameters.

g. Event rates:

The rates $\sigma(\gamma\gamma \to h) \times \mathrm{BR}(h \to b\bar{b})$ and $\sigma(\gamma\gamma \to h) \times \mathrm{BR}(h \to \mathrm{WW}^*)$ are directly measured at the $\gamma\gamma$ collider. In the MSSM, these rates are generally expected to deviate from their SM predictions. This leads to additional sensitivity to the possible MSSM nature of a light Higgs boson, and a full analysis of these deviations should be performed. In particular, if the production cross section and/or either of the decay rates are suppressed compared to their SM values, the statistical precision of the $\gamma\gamma$ collider measurements may suffer.

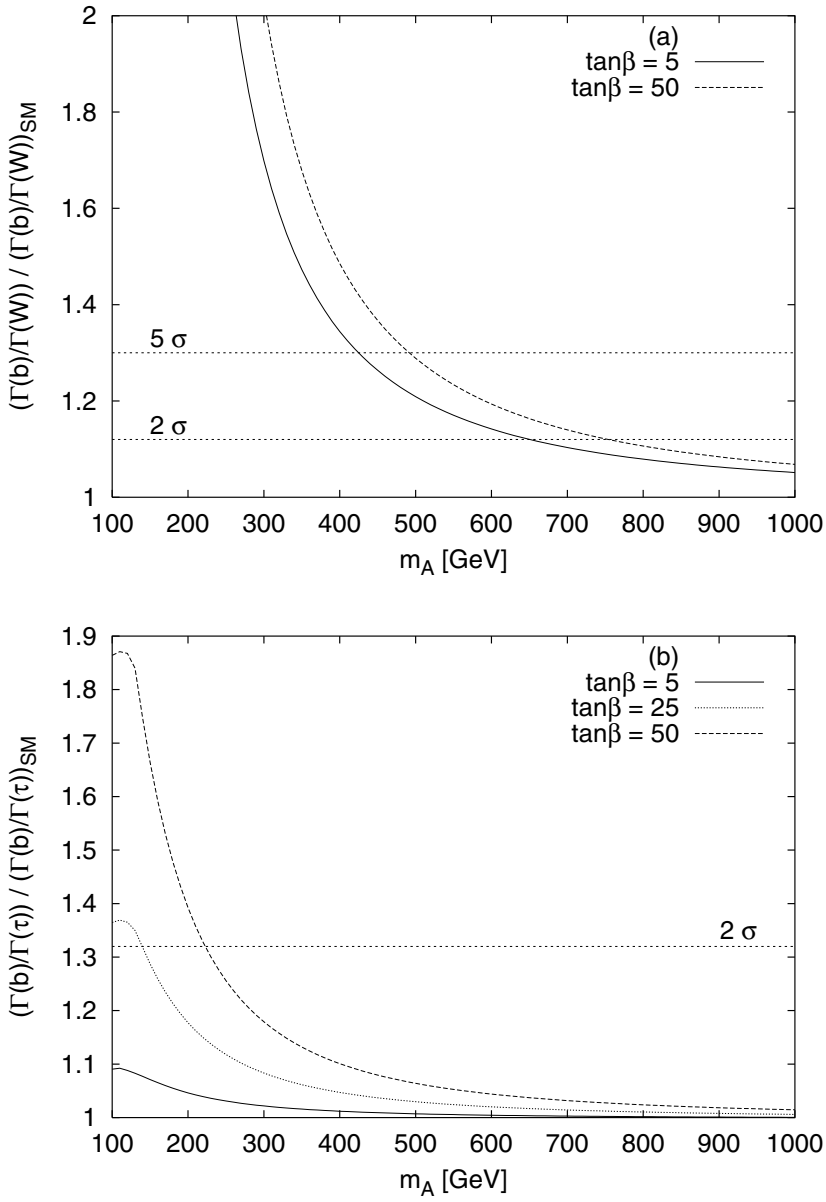

Figure 8: (a) $\Gamma(h \to b\bar{b})/\Gamma(h \to \mathrm{WW}^*)$ in the MSSM normalized to its SM value. We exhibit 2σ and 5σ deviations based on a 6% measurement. (b) $\Gamma(h \to b\bar{b})/\Gamma(h \to \tau\tau)$ in the MSSM normalized to its SM value. The 2σ deviation shown is based on a 16% measurement. The MSSM parameters are $M_{\tilde{Q}} = M_{\tilde{U}} = M_{\tilde{g}} = 1$ TeV, $M_2 = 2M_1 = -\mu = 200$ GeV, $X_t \equiv A_t - \mu \cot\beta = \sqrt{6}M_{\tilde{Q}}$, and $A_b = A_t$ (i.e., a maximal mixing scenario). Numerical results are obtained from HDECAY [17] with the Δ_b corrections added.

3.3. CP violation in Higgs couplings

CP violation in Higgs couplings has been previously considered at $\gamma\gamma$ colliders in [25, 26]; these analyses require linearly polarized initial-state photons [25] or interference of final-state fermions with the continuum in $\gamma\gamma \to H \to t\bar{t}$ [26]. These analyses probe CP violation in the Higgs couplings to $\gamma\gamma$ and $t\bar{t}$ pairs, respectively. As pointed out in [27], CP violation measurements in Higgs production and decay probe both CP mixing in the Higgs mass eigenstate and CP violation in the Higgs couplings to external particles. Thus CP violation measurements in many different Higgs couplings are desirable.

Here we consider observables that probe CP violation in the Higgs coupling to W boson pairs. We make no assumptions about the photon polarization, so that this study can be done with a $\gamma\gamma$

collider running as a Higgs factory, as described before. Our CP-odd observables are constructed in such a way that they are directly measurable in experiment without reconstruction of the W boson rest frames or the center-of-momentum frame of the initial pair of photons. Thus they can be measured using semileptonic W decays, despite the unknown momentum carried off by the neutrinos.

We consider the process $\gamma\gamma \to H \to W^+W^-$. We assume that the polarization of the initial photons is not known. Then, a CP test in this mode is possible only if the polarizations of the W^+ or W^- are observed. To obtain information about the polarizations we consider leptonic decays of the W bosons:

$$\gamma(p_1) + \gamma(p_2) \to H \to W^+(k_1) + W^-(k_2) \to \ell^+(q_1) + \ell^-(q_2) + \text{neutrinos}, \tag{3}$$

where all the momenta are defined in the $\gamma\gamma$ c.m. frame. The process $\gamma\gamma \to H \to W^+W^-$ proceeds with an amplitude

$$T_{fi} = \varepsilon_{\nu_1}(p_1)\varepsilon_{\nu_2}(p_2)\varepsilon^*_{\mu_1}(k_1)\varepsilon^*_{\mu_2}(k_2)A^{\nu_1\nu_2\mu_1\mu_2}(p_1,p_2,k_1,k_2). \tag{4}$$

For the decay process $W^+(k_1) \to \ell^+(q_1) + \nu$ we define a covariant decay matrix $\rho^+_{\mu\nu}(k_1,q_1)$ and similarly for the W^- decay matrix $\rho^-_{\mu\nu}(k_2,q_2)$. The probability for the process in (3) may be written as:

$$R(\mathbf{p_1},\mathbf{k_1},\mathbf{q_1},\mathbf{q_2}) = \frac{1}{4}A^{\nu_1\nu_2\mu_1\mu_2}(p_1,p_2,k_1,k_2)A^*_{\nu_1\nu_2}{}^{\mu_1'\mu_2'}(p_1,p_2,k_1)\rho^+_{\mu_1\mu_1'}(k_1,q_1)\rho^-_{\mu_2\mu_2'}(k_2,q_2). \tag{5}$$

If CP invariance holds, then $R(\mathbf{p_1},\mathbf{k_1},\mathbf{q_1},\mathbf{q_2}) = R(\mathbf{p_1},\mathbf{k_1},-\mathbf{q_2},-\mathbf{q_1})$.

The expectation value of any observable O that is a function of $\mathbf{p_1},\mathbf{k_1},\mathbf{q_1}$ and $\mathbf{q_2}$ can be obtained from

$$\langle O\rangle = \frac{1}{N}\int f_\gamma(x_1)f_\gamma(x_2)\frac{dx_1dx_2}{x_1x_2}\frac{\beta}{2(4\pi k_1^0)^4}\int d\Omega\frac{d\Omega_1}{(1-\beta\hat{\mathbf{k}}_1\cdot\hat{\mathbf{q}}_1)^2}\frac{d\Omega_2}{(1+\beta\hat{\mathbf{k}}_1\cdot\hat{\mathbf{q}}_2)^2}OR(\mathbf{p_1},\mathbf{k_1},\mathbf{q_1},\mathbf{q_2}), \tag{6}$$

normalized so that $\langle 1\rangle = 1$. Here, $d\Omega$, $d\Omega_1$ and $d\Omega_2$ are the solid angle of $\mathbf{k_1}$, $\mathbf{q_1}$ and $\mathbf{q_2}$, respectively, and $f_\gamma(x)$ gives the proportion of the photons with the fraction x of the initial electron or positron beam energy. Experimental cuts can be included in (6), but for our purpose they must be CP blind.

The momenta $\mathbf{p_1}$, $\mathbf{k_1}$, $\mathbf{q_1}$ and $\mathbf{q_2}$ are not directly measurable due to the missing neutrinos and the lack of knowledge about the $\gamma\gamma$ c.m. frame. To construct CP-odd observables, we use the lepton momenta, which are directly measured in experiment and are related to $\mathbf{q_1}$ and $\mathbf{q_2}$ through a Lorentz boost. We denote these momenta by $q_+ = (E_+,\mathbf{q}_+)$ and $q_- = (E_-,\mathbf{q}_-)$ for ℓ^+ and ℓ^-, respectively. We construct the following CP odd observables:

$$\begin{aligned} O_1 &= \frac{E_+ - E_-}{M_W}, \\ O_2 &= (\hat{\mathbf{p}}\cdot\hat{\mathbf{q}}_+)^2 - (\hat{\mathbf{p}}\cdot\hat{\mathbf{q}}_-)^2, \\ O_3 &= \hat{\mathbf{p}}\cdot(\hat{\mathbf{q}}_+ - \hat{\mathbf{q}}_-)\hat{\mathbf{p}}\cdot(\hat{\mathbf{q}}_+\times\hat{\mathbf{q}}_-), \end{aligned}$$

with $\hat{\mathbf{q}}_+ = \mathbf{q}_+/|\mathbf{q}_+|$, $\hat{\mathbf{q}}_- = \mathbf{q}_-/|\mathbf{q}_-|$, and the vector $\hat{\mathbf{p}}$ is the direction of motion of the electron or positron. Because of the Bose symmetry of the two-photon initial state, the expectation value of any observable which is odd in $\hat{\mathbf{p}}$ is zero. With these observables one can also define the corresponding CP asymmetries:

$$A_i = \frac{N(O_i>0) - N(O_i<0)}{N(O_i>0) + N(O_i<0)}, \qquad (i=1,2,3) \tag{7}$$

where $N(O_i>0)$ ($N(O_i<0)$) denotes the number of events with $O_i>0$ ($O_i<0$). Any nonzero $<O_i>$ or any nonzero A_i indicates CP violation. Further, the observables O_1 and O_2 are CPT odd, the expectation values of them and the corresponding asymmetries can be nonzero only if an absorptive part of the amplitude and CP violation exist.

Summarizing, CP-odd observables and the corresponding CP asymmetries for the process $\gamma\gamma \to H \to WW$ can be constructed from the directly measured energies and momenta of the leptons

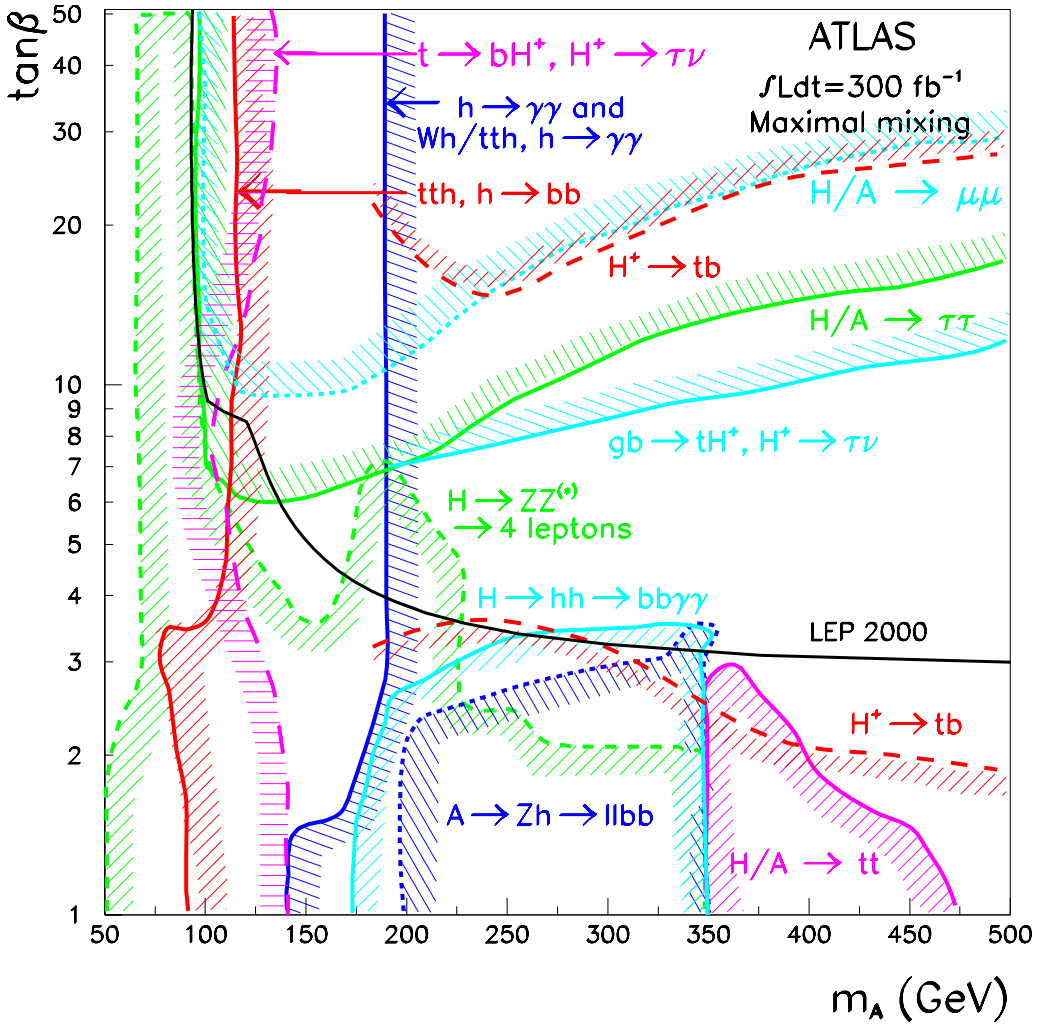

Figure 9: 5σ *discovery contours for MSSM Higgs boson detection at the LHC in various channels, assuming maximal mixing and an integrated luminosity of* $L = 300\,\text{fb}^{-1}$ *for the ATLAS detector. This figure is preliminary [30].*

from the W decays. With these observables one can detect CP violation without requiring complete knowledge of the center-of-momentum frame of the initial photons or of the rest frame of the W bosons. Therefore, our observables are easy to measure on an event-by-event basis. An estimate gives a statistical error of $\delta A/A \sim 5\%$ or better from the measurements that could be made at CLICHE, see section 3.3.1.

3.4. The Heavy MSSM Higgs Bosons H^0, A^0

In many scenarios, it is likely that we will observe small deviations from SM expectations in precision measurements of the properties of the SM-like Higgs boson, and thus suspect the presence of heavy Higgs bosons. However, direct production of the heavier Higgs bosons in e^+e^- collisions is likely to require large machine energy. For example, in the MSSM, $e^+e^- \to H^0, A^0$ is the most relevant process in the decoupling limit, but requires $\sqrt{s} > m_{H^0} + m_{A^0}$, with $m_{H^0} + m_{A^0} \sim 2m_{A^0}$ as the decoupling limit sets in. The alternative modes $e^+e^- \to b\bar{b}H^0, b\bar{b}A^0$ are only viable if $\tan\beta$ is large [29]. At the LHC, either low or high $\tan\beta$ is required for discovery of H^0, A^0 if they have mass $\gtrsim 250\,\text{GeV}$, as seen in Figure 9. After accumulation of $L = 300\,\text{fb}^{-1}$ at the LHC, H^0, A^0 will be H^0, A^0 will be detected except in the wedge of parameter 250 GeV and moderate $\tan\beta$, where only h^0 can be detected. If the e^+e^- LC is operated at $\sqrt{s} = 630\,\text{GeV}$, then detection of $e^+e^- \to H^0A^0$

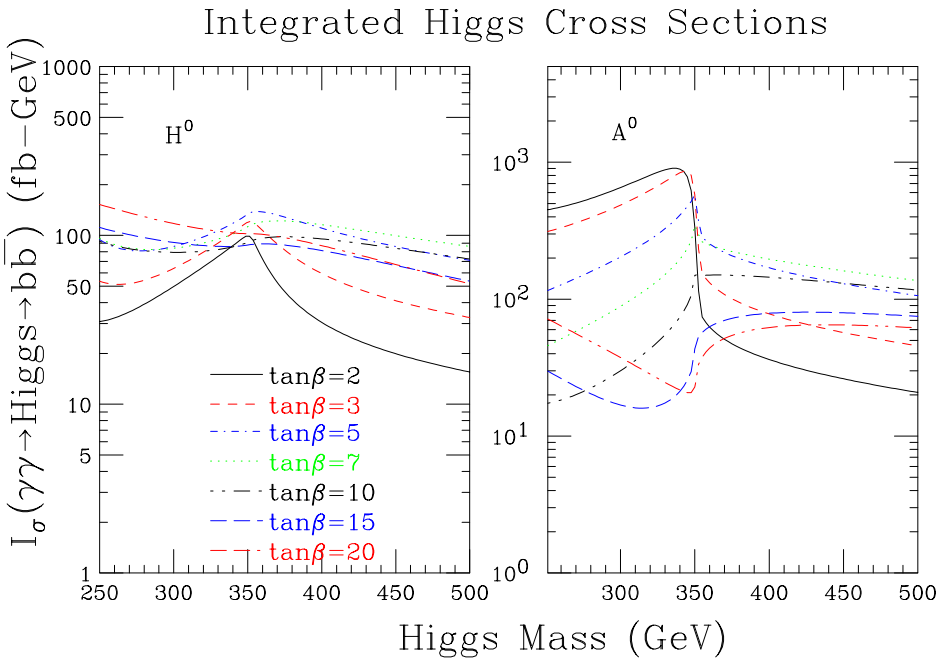

Figure 10: Integrated H^0 and A^0 Higgs cross sections as defined in [18] as a function of m_{A^0}, for a variety of $\tan\beta$ values. We assume the maximal-mixing scenario with $m_{\rm SUSY} = 1$ TeV. Supersymmetric particle loops are neglected.

will be possible for $m_{A^0} \sim m_{H^0}$ up to nearly 300 GeV. In this case, some other means of detecting H^0, A^0 must be found in the portion of the LHC wedge with $m_{A^0} \gtrsim 300$ GeV.

We show here that single H^0, A^0 production via $\gamma\gamma$ collisions will allow their discovery throughout a large fraction of this wedge: see [18] for details. The event rate can be substantial due to quark loop contributions (t and, at high $\tan\beta$, b) and loops containing SUSY particles. In this study, we assume that the masses of the superparticles (charginos, squarks, sleptons, etc.) are sufficiently heavy that H^0, A^0 do not decay to them and that the superparticle loop contributions to the $\gamma\gamma(H^0, A^0)$ couplings are negligible.

If we have no reliable prior constraints on m_{A^0}, m_{H^0}, an important question is whether it is best to search for the H^0, A^0 by scanning in $\sqrt{s}$ (and thereby in $E_{\gamma\gamma}$) using a peaked spectrum, or running at fixed $\sqrt{s}$ using a broad $E_{\gamma\gamma}$ spectrum part of the time and a peaked spectrum the rest of the time [28]. Our results indicate that if covering the LHC wedge region is the goal, then running at a single energy, half the time with a peaked $E_{\gamma\gamma}$ luminosity distribution and half the time with a broad distribution, is likely to be the optimal approach.

The effective integrated cross sections for $\gamma\gamma \to H^0, A^0 \to b\bar{b}$, taking into account acceptance and cuts, are plotted as a function of m_{A^0} for a variety of $\tan\beta$ values in Figure 10 (see [18] for details). Numerical results were obtained using HDECAY [17], with $m_t = 175$ GeV, $m_{\rm SUSY} = 1$ TeV for all slepton and squark soft-SUSY-breaking masses and $\mu = +1$ TeV. We also assume the maximal-mixing scenario, $A_t = \mu/\tan\beta + \sqrt{6} m_{\rm SUSY}$, and $A_b = A_\tau = A_t$. If the LC is operated at $\sqrt{s} = 630$ GeV (corresponding to $x \sim 5.69$ for 1 micron laser wavelength) we can potentially probe Higgs masses up to ~ 500 GeV.

The photon energy and polarization spectra are computed using the CAIN [14] Monte Carlo. For the broad spectrum, the luminosity remains quite large even below the $E_{\gamma\gamma}$ peak at $E_{\gamma\gamma} = 500$ GeV, and the polarization combination $\langle\lambda\lambda'\rangle$ is large for $E_{\gamma\gamma} > 450$ GeV. For the peaked spectrum, the luminosity is substantial for $E_{\gamma\gamma} = 400$ GeV and rises rapidly with decreasing $E_{\gamma\gamma}$. In addition, reasonably large $\langle\lambda\lambda'\rangle$ is retained for $250 < E_{\gamma\gamma} < 400$ GeV. However, in both cases, $1 - \langle\lambda\lambda'\rangle$ is always large enough that the $J_z = 2$ part of the $b\bar{b}$ background will be dominant. In order to detect the Higgs bosons with mass substantially below the machine energy of 630 GeV, we must employ cuts that remove as little luminosity for $E_{\gamma\gamma}$ substantially below $\sqrt{s}$ as possible while still eliminating most of the $b\bar{b}(g)$ and $c\bar{c}(g)$ backgrounds. A cut on $|\cos\theta^*| < 0.5$ (where θ^* is the angle of the b jets in the $\gamma\gamma$ rest frame) eliminates much of the (t-channel) background

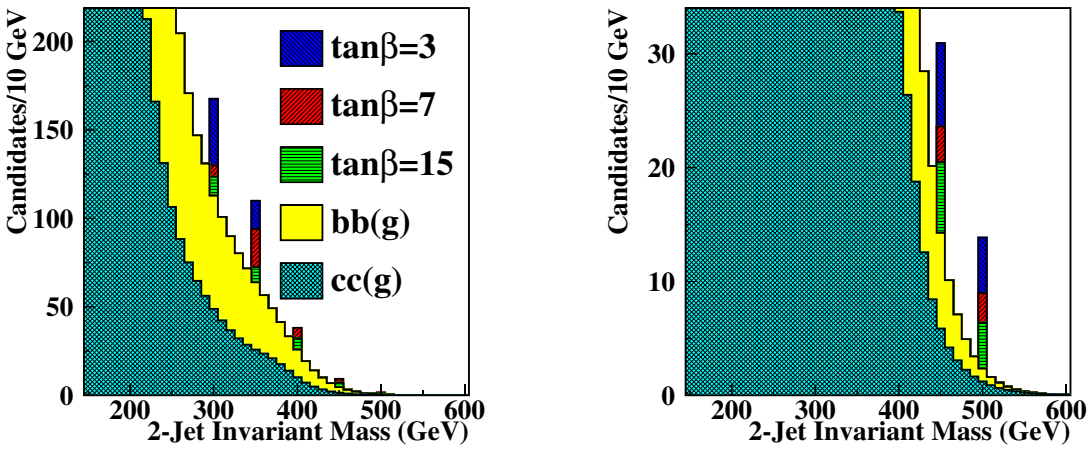

Figure 11: Signal and background rates for the $[m_{A^0}, \tan\beta]$ cases considered for (a) broad spectrum and (b) peaked spectrum operation at $\sqrt{s} = 630$ GeV for one year (10^7 sec). The signals shown assume that 50% of the total number of signal events fall into the single 10 GeV bin shown. Signals in the side bins are not shown.

while decreasing the (s-channel) signal by only a factor of two. A second cut is imposed upon the $m_{b\bar{b}}$ mass distribution. The optimal value for this cut depends upon the Higgs widths, the degree of degeneracy of the H^0 and A^0 masses, and the detector resolutions and reconstruction techniques. For the $\tan\beta$ range inside the problematical wedge ($15 > \tan\beta > 3$), the A^0 and H^0 are still relatively narrow, with widths below 1–2 GeV. Thus, the width of the $b\bar{b}$ mass distribution derives mostly from detector resolutions and reconstruction procedures. A full Monte Carlo analysis for heavy Higgs bosons with relatively small widths is not yet available. However, there are many claims in the literature that the resulting mass resolution will almost certainly be better than $30\%/\sqrt{m_{b\bar{b}}}$ (the result obtained assuming $18\%/\sqrt{E_{jet}}$ for each of the b jets) [3, 4, 7]. Very roughly, this corresponds to a full-width at half maximum of about 6 GeV in the mass range from 250–500 GeV of interest. We adopt the procedure of considering a 10 GeV bin centered on the Higgs mass in question and assume that 50% of the Higgs events will fall into this bin. This would be very conservative for the 6 GeV full-width estimate *assuming that the H^0 and A^0 are degenerate in mass.* In practice, they are not exactly degenerate and so we have used the 10 GeV as a conservative approach to allowing for this non-degeneracy.

The resulting signals and backgrounds after cuts are shown in Figure 11 as a function of 2-jet invariant mass with the signals superimposed (we plot only the central 10 GeV bin assumed to contain 50% of the signal events). Results for different values of $\tan\beta$ and m_{A^0} are shown for running in the broad and peaked spectra configurations. Note that for the $m_{A^0} = 350$ GeV points, we have conservatively run HDECAY so that m_{H^0}, m_{A^0} are slightly above the $t\bar{t}$ threshold. As can be seen from Figure 10, the rates (especially that for $\gamma\gamma \to A^0 \to b\bar{b}$) depend sensitively on the Higgs masses relative to the $t\bar{t}$ threshold. For m_{A^0} just below the plotted 350 GeV points, the net signal is much stronger.

Many of the $[m_{A^0}, \tan\beta]$ cases considered will yield an observable 4σ signal. Our ability to cover the LHC wedge in Our ability to cover the LHC wedge in which the neutral H^0, A^0 Higgs illustrated in Figure 12. (The $H^\pm$ can be detected at the LHC down to lower $\tan\beta$ values than can the H^0, A^0, as shown in Figure 9.) After running for two years in the broad spectrum configuration, 7 of the 13 $[m_{A^0}, \tan\beta]$ cases considered in the LHC wedge region with $m_{A^0} = 300, 350, 400$ GeV will yield a 4σ or greater Higgs signal, with the best sensitivity at low to moderate $\tan\beta$. Similarly, after running for one year in the peaked spectrum configuration, 7 of the 10 $[m_{A^0}, \tan\beta]$ cases considered in the LHC wedge with $m_{A^0} = 450, 500$ GeV will yield a 4σ or greater Higgs signal, with the best sensitivity at moderate to high $\tan\beta$. These points are shown in Figure 12(b). The areas of parameter space covered by the broad spectrum and the peaked spectrum running are

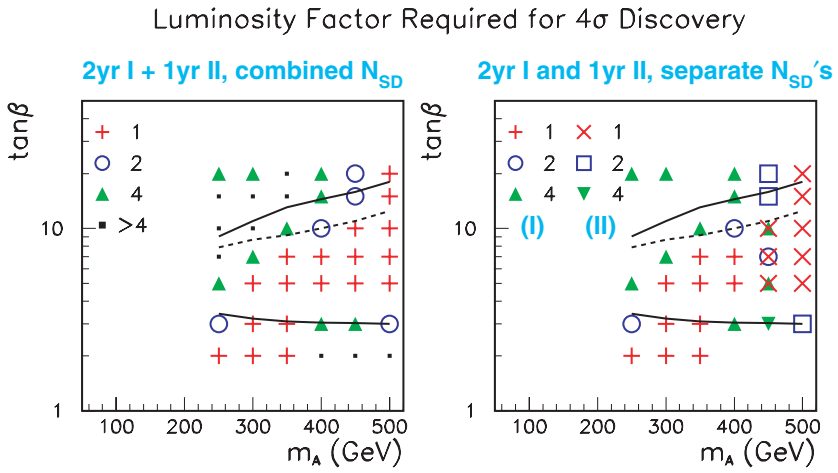

Figure 12: The $[m_{A^0}, \tan\beta]$ points for which two years of broad spectrum operation plus one year of peaked spectrum operation at $\sqrt{s} = 630\,\text{GeV}$ will yield $S/\sqrt{B} \geq 4$. Shown are (a) the combined significance from both the broad spectrum and peaked spectrum running and (b) the separate significances from the broad spectrum and peaked spectrum running. Also shown are the additional points for which a 4σ signal is achieved if the total luminosity is doubled ('2') or quadrupled ('4') relative to our assumed luminosity. Such luminosity increases could be achieved by improved technical designs and/or longer run times; e.g., the luminosity expected from the TESLA design corresponds roughly to the doubled luminosity ('2'). The small black squares in (a) indicate additional points sampled for which even a luminosity increase by a factor of four for both spectra does not yield a 4σ signal. The solid curves show the boundaries of the LHC wedge region from Fig. 9 — the lower black curve is that from the LEP (maximal-mixing) limits, but is somewhat higher than that currently claimed by the LEP electroweak working group. For $\tan\beta$ values above the dashed curve, $H^\pm \to \tau^\pm \nu_\tau$ can be directly detected at the LHC.

complementary; if data from both broad spectrum and peaked spectrum running are combined for a given parameter space point, the statistical significance is only slightly improved. In all, a 4σ or greater Higgs signal would be detected for 15 of the 23 points considered in the LHC wedge, a coverage of about 65%. Further improvements in luminosity or mass resolution would be helpful for guaranteeing complete coverage of the wedge region. If the luminosity is doubled for both the broad spectrum and peaked spectrum running, the coverage increases to 78%. In addition, for $\sqrt{s} = 630\text{GeV}$ it is very probable that one could see $e^+e^- \to H^0A^0$ pair production for $m_{A^0} = 300\text{GeV}$, in which case $\gamma\gamma$ operation with doubled luminosity would allow detection of H^0, A^0 throughout most of the remaining portion of the wedge in which they cannot be seen by other means (see Figure 12(b)). We also note that in this study we have considered only $b\bar{b}$ final states. At low $\tan\beta$, we expect that the $H^0 \to h^0h^0$ and $A^0 \to Zh^0$ channels will provide observable signals for the remaining points with $m_{A^0} \leq 2m_t = 350\,\text{GeV}$ in the LHC wedge. The $t\bar{t}$ channels might provide further confirmation for $b\bar{b}$ signals for wedge points with $m_{A^0} > 450\,\text{GeV}$. Finally, we note that the single most difficult wedge point considered is $m_{A^0} = 400, \tan\beta = 15$, which is at the edge of the LHC wedge. The region of the LHC wedge in which our running scenario would not enable H^0, A^0 detection in $\gamma\gamma$ collisions is roughly given by $325\,\text{GeV} \lesssim m_{A^0} \lesssim 400\text{GeV}$ and $\tan\beta > 8$. In this region, though, the LHC would be able to detect the charged Higgs boson via $H^\pm \to \tau^\pm\nu_\tau$ (see Figure 9) and measure its mass to about $\pm 25\,\text{GeV}$. If studies of the sparticles indicate that the MSSM is the correct theory, then we would expect $m_{A^0} \sim m_{H^0} \sim m_{H^\pm}$, and could then run the $\gamma\gamma$ collider with a peaked spectrum at the $\sqrt{s}$ value yielding $E_{\text{peak}} \sim m_{H^\pm}$.

A rough determination of $\tan\beta$ is likely to be possible using the data associated with the initial discovery of H^0, A^0 in $\gamma\gamma$ collisions. We show the approximate fractional error on $\tan\beta$ from the initial discovery data for the $[m_{A^0}, \tan\beta]$ points studied in Table II. Although the errors are not small, this determination can be fruitfully combined with other $\tan\beta$ determinations, especially for larger $\tan\beta$ values where other techniques for determining $\tan\beta$ also have substantial errors. More importantly, these results show clearly that a dedicated measurement of the $\gamma\gamma \to H^0, A^0 \to b\bar{b}$ rate and the rates in other channels ($H^0 \to h^0h^0$, $A^0 \to Zh^0$, $H^0, A^0 \to t\bar{t}$) using a peaked spectrum with $E_{\text{peak}} = m_{A^0}$ is likely to yield a rather high precision determination of $\tan\beta$ after

several years of optimized operation, and may provide information about other supersymmetry parameters.

Table II Approximate uncertainties in $\tan\beta$ as determined from measurements of the $\gamma\gamma \to H^0, A^0 \to b\bar{b}$ rate associated with Higgs discovery in the LHC wedge. These errors assume two years of operation in broad spectrum mode and one year of operation in peaked spectrum mode at $\sqrt{s} = 630$ GeV. Errors larger than 100% are not shown.

m_{A^0} (GeV)	250	300	350	400	450	500
$\tan\beta = 2$	0.51	0.34	0.20	0.66	0.46	0.48
$\tan\beta = 3$	0.51	0.27	–	0.45	0.30	0.32
$\tan\beta = 5$	0.71	0.34	0.19	–	0.56	0.55
$\tan\beta = 7$	–	0.66	0.23	0.62	0.67	0.87
$\tan\beta = 10$	–	–	0.50	0.64	0.46	0.53
$\tan\beta = 15$	0.46	0.67	–	–	–	–

4. $e\gamma$ collider option—doubly charged Higgs bosons

Doubly charged Higgs bosons would have a distinct experimental signature. Such particles arise in many extensions of the Standard Model (SM) such as the Higgs triplet model of Gelmini and Roncadelli [31] and the left–right symmetric model. The signals for doubly charged Higgs bosons arising from an $SU(2)_L$ triplet were studied in the process $e^-\gamma \to e^+\mu^-\mu^-$. Details of the analysis are given in reference [32] and contribution P3-18 of these proceedings. The photon was assumed to be produced by backscattering a laser from the e^+ beam of an e^+e^- collider [33]. We consider e^+e^- center of mass energies of $\sqrt{s} = 500$, 800, 1000, and 1500 GeV appropriate to the TESLA/NLC/JLC high energy colliders and $\sqrt{s} = 3$, 5, and 8 TeV for the CLIC proposal. In all cases an integrated luminosity of $\mathcal{L} = 500$ fb^{-1} was assumed. Because the signature of same sign muon pairs in the final state is so distinctive, with no SM background, the process can be sensitive to virtual Δ^{--}'s with masses in excess of the center of mass energy, depending on the strength of the Yukawa coupling to leptons.

Indirect constraints on Δ masses and couplings have been obtained from lepton number violating processes [34]. Rare decay measurements [35] yield very stringent restrictions on the non-diagonal couplings $h_{e\mu}$ which were consequently neglected. Stringent limits on flavor diagonal couplings come from the muonium anti-muonium conversion measurement [36] which requires that the ratio of the Yukawa coupling, h, and Higgs mass, M_Δ, satisfy $h/M_\Delta < 0.44$ TeV^{-1} at 90% C.L.. These bounds allow the existence of low-mass doubly charged Higgs with a small coupling constant. Direct search strategies for the Δ^{--} have been explored for hadron colliders [37], with the mass reach at the LHC extending to ~ 850 GeV. Signatures have also been explored for various configurations of lepton colliders, including $e\gamma$ colliders.

In the process $e^-\gamma \to e^+\mu^-\mu^-$, the signal of like-sign muons is distinct and SM background free, offering excellent potential for doubly charged Higgs discovery. The process proceeds via the production of a positron along with a Δ^{--}, with the subsequent Δ decay into two muons as well as through additional non-resonant contributions. Due to contributions to the final state that proceed via s-channel Δ^{--}'s, the doubly-charged Higgs boson width must be included. Because the Δ width is model dependent, we account for the possible variation in width without restricting ourselves to specific scenarios by calculating the width using $\Gamma(\Delta^{--}) = \Gamma_b + \Gamma_f$ where Γ_b is the partial width to final state bosons and Γ_f is the partial width into final state fermions. Two scenarios for the bosonic width were considered: a narrow width scenario with $\Gamma_b = 1.5$ GeV and a broad width scenario with $\Gamma_b = 10$ GeV. These choices represent a reasonable range for various values of the masses of the different Higgs bosons. The partial width to final state fermions is given by $\Gamma(\Delta^{--} \to \ell^-\ell^-) = 1/(8\pi)h^2_{\ell\ell}M_\Delta$. Since we assume $h_{ee} = h_{\mu\mu} = h_{\tau\tau} \equiv h$, we have $\Gamma_f = 3 \times \Gamma(\Delta^{--} \to \ell^-\ell^-)$.

We consider two possibilities for the Δ^{--} signal. We assume that either all three final state particles are observed and identified or that the positron is not observed, having been lost down the beam pipe. To take into account detector acceptance we restrict the angles of the observed

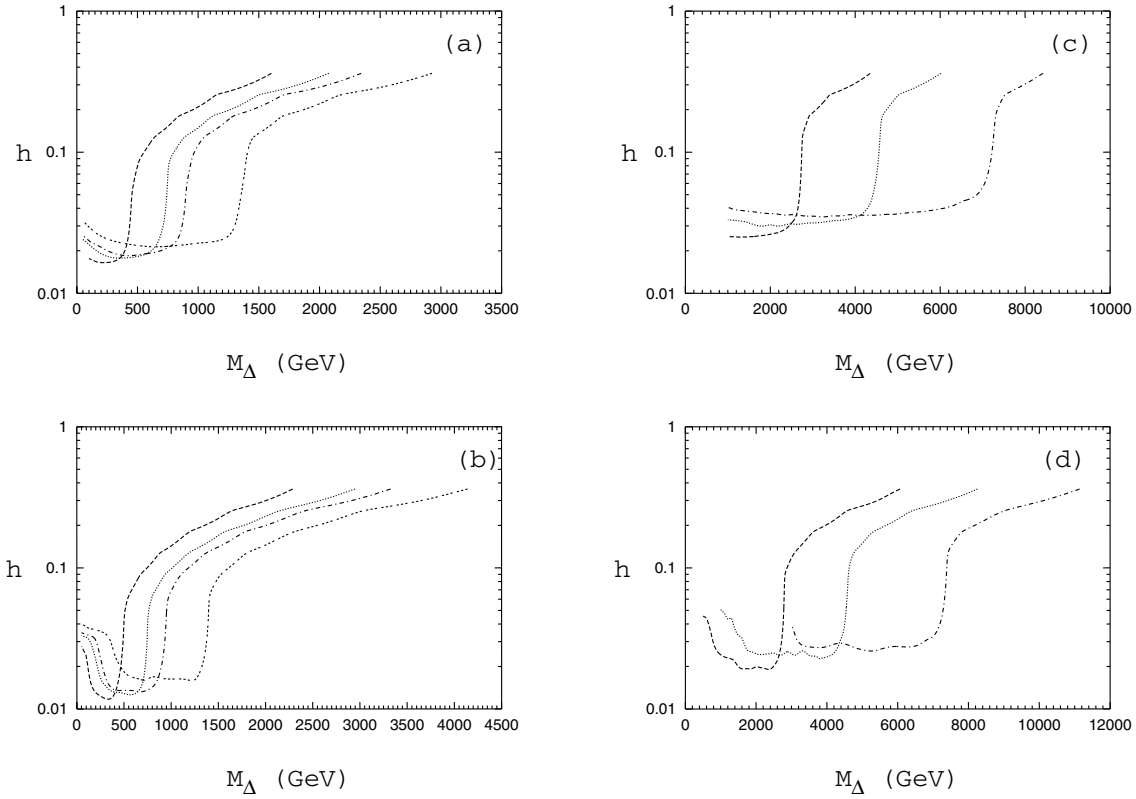

Figure 13: Discovery limits for the charged Higgs bosons as a function of Yukawa coupling and M_Δ. (a) and (b) show TESLA/NLC/JLC center of mass energies $\sqrt{s}$ = 500, 800, 1000, and 1500 GeV, for the three particle and two particle final states, respectively. (c) and (d) show CLIC center of mass energies $\sqrt{s}$ = 3, 5, and 8 TeV, for the three particle and two particle final states, respectively.

particles relative to the beam, θ_μ, θ_{e^+}, to the ranges $|\cos\theta| \leq 0.9$. We restrict the particle energies E_μ, $E_{e^+} \geq 10$ GeV and assumed an identification efficiency for each of the detected final state particles of $\varepsilon = 0.9$.

Given that the signal for doubly charged Higgs bosons is so distinctive and SM background free, discovery would be signalled by even one event. Because the value of the cross section for the process we consider is rather sensitive to the Δ width, the potential for discovery of the Δ is likewise sensitive to this model dependent parameter. Varying Γ_b, we find that, relative to $\Gamma_b = 10$ GeV, the case of zero bosonic width has a sensitivity to the Yukawa coupling h which is greater by a factor of about 5 [32].

In Figure 13 we show 95% probability (3 event) contours in the $h - M_\Delta$ parameter space. In each case, we assume the narrow width $\Gamma = 1.5 + \Gamma_f$ GeV case. Figure 1a corresponds to the center of mass energies $\sqrt{s}$ = 500, 800, 1000, and 1500 GeV, for the case of three observed particles in the final state, whereas Fig. 1b shows the case where only the two muons are observed. Figs. 1c and 1d correspond to the energies being considered for the CLIC e^+e^- collider, namely, $\sqrt{s}$ = 3, 5, and 8 TeV, for the three body and two body final states, respectively. In each case, for $\sqrt{s}$ above the Δ production threshold, the process is sensitive to the existence of the Δ^{--} with relatively small Yukawa couplings. However, when the M_Δ becomes too massive to be produced the values of the Yukawa couplings which would allow discovery grow larger slowly.

The observation of doubly charged Higgs bosons would represent physics beyond the SM and, as such, searches for this type of particle should be part of the experimental program of any new high energy facility. We found that for $\sqrt{s_{e\gamma}} > M_\Delta$ doubly charged Higgs bosons could be discovered for even relatively small values of the Yukawa couplings; $h > 0.01$. For larger values of the Yukawa coupling the Δ should be produced in sufficient quantity to study its properties. For values of M_Δ greater than the production threshold, discovery is still possible due to the distinctive, background free final state in the process $e\gamma \to e^+\mu^-\mu^-$ which can proceed via virtual contributions from intermediate Δ's. Thus, even an e^+e^- linear collider with modest energy has

the potential to extend Δ search limits significantly higher than can be achieved at the LHC.

5. Conclusions

Our working group devoted most of its effort to exploring the various ways in which a $\gamma\gamma$ collider could contribute to our understanding of Higgs physics.

For a SM-like Higgs boson, it will be possible to determine $\Gamma(\gamma\gamma \to h)B(h \to b\bar{b})$, $\Gamma(\gamma\gamma \to h)B(h \to \mathrm{WW})$ and $\Gamma(\gamma\gamma \to h)B(h \to \gamma\gamma)$ with excellent precision, e.g. ~ 2, 5 and 8%, respectively, for a $m_h \sim 115\,\mathrm{GeV}$. In addition, the Higgs mass can be measured three ways (fitting the peaks in the $\bar{b}b$ and $\gamma\gamma$ mass distributions, and by the threshold method), and the partial width $\Gamma_{\gamma\gamma}$ can be extracted on the basis of a measurement of $\mathcal{B}r(H \to \bar{b}b)$ from an e^+e^- machine to very good accuracy, not matched by any other method. At this level of accuracy, deviations that might be present as the result of the SM-like Higgs boson being part of a larger Higgs sector, such as that of the MSSM, would be visible if some of the other Higgs bosons were not too much heavier than 500 GeV or so. The WW decay mode will allow us to make a 5% measurement of asymmetries that are sensitive to the CP of the Higgs. In addition, a determination of the CP nature of any Higgs boson can also be observed by employing transversely (linearly) polarized laser beam photons [8, 18].

For the purpose of building a light Higgs factory, the optimal operating conditons are found to be when we operate at the peaked $E_{\gamma\gamma}$ spectrum, that is obtained with lower electron beam energy ($E = 75 - 80$ GeV) combined with a frequency tripler to reduce the wavelength of the available high power 1 micron lasers.

For the higher energy $\gamma\gamma$ collider, we conclude that it will be possible to detect A^0, H^0 of the MSSM Higgs sector using just $b\bar{b}$ states in a large fraction of the wedge of moderate-$\tan\beta$ space beginning at $m_{A^0} \gtrsim 300\,\mathrm{GeV}$ (the approximate upper reach of the $e^+e^- \to H^0, A^0$ pair production process for $\sqrt{s} = 630\,\mathrm{GeV}$) up to the $E_{\gamma\gamma}$ spectrum limit of about 500 GeV, by running for two years with a broad spectrum and one year with a peaked spectrum, without lowering the energy below $\sqrt{s} = 630\,\mathrm{GeV}$. By also considering $H^0 \to h^0h^0$, $A^0 \to Zh^0$ and $H^0, A^0 \to t\bar{t}$ final states, we estimate that somewhat more than 85% of the wedge parameter region with $m_{A^0} \lesssim 500\mathrm{GeV}$ would provide a detectable signal after a total of two to three years of operation. Further, at all of the higher $\tan\beta$ points in the wedge region for which $\gamma\gamma$ collisions would not allow detection of the H^0, A^0, detection of $H^\pm \to \tau^\pm\nu_\tau$ would be possible at the LHC. Then, using the MSSM prediction $m_{A^0} \sim m_{H^0} \sim m_{H^\pm}$ for $m_{A^0} \gtrsim 200\,\mathrm{GeV}$, one could optimize the search for H^0, A^0 at the $\gamma\gamma$ collider by running with a peaked luminosity spectrum with $E_{\mathrm{peak}} = m_{H^\pm}$. Thus, by combining $\gamma\gamma$ collider operation at $\sqrt{s} = 630\,\mathrm{GeV}$ with e^+e^- running and LHC searches for the MSSM Higgs bosons, it would be essentially guaranteed that we could detect all the neutral Higgs bosons of the MSSM Higgs sector if they have mass $\lesssim 500\,\mathrm{GeV}$, whereas without the $\gamma\gamma$ collider one would detect only the h^0 at both the LC and LHC in the LHC wedge for $m_{A^0} \gtrsim 300\,\mathrm{GeV}$. One caveat to this very optimistic set of conclusions is that if supersymmetric particles are light enough to be produced in H^0, A^0 decays, they will alter the $\gamma\gamma \to H^0, A^0$ cross sections and reduce the $H^0, A^0 \to b\bar{b}$ branching ratios, especially at low $\tan\beta$. In short, if we detect supersymmetric particles at the LHC and LC consistent with the MSSM structure and find only the h^0 at the LHC and LC, $\gamma\gamma$ operation focusing on Higgs discovery will be a high priority.

References

[1] See http://diablo.phys.nwu.edu/~mvelasco/gg-papers.html.
[2] E3-SO2, Linear Colliders—Special Option $\gamma\gamma$ and $e\gamma$ ollisions.
[3] NLC Collaboration, *2001 Report on the Next Linear Collider: A Report Submitted to Snowmass 2001*, SLAC-R-571, FERMILAB-CONF-01-075-E, LBNL-PUB-47935, UCRL-ID-144077, Jun 2001, and SLAC-R-570.
[4] K. Abe *et al.*, hep-ph/0109166.
[5] The CLIC Study Team, G. Guignard (ed.), *A 3 TeV Linear Collider Based on CLIC Technology*, CERN 2000-008.
[6] D. Asner, et al., "Higgs Physics with a $\gamma\gamma$ Collider Based on CLIC1", CERN-TH/2001-235, BNL-HET/01-32, Oct. 2001, *To be Submitted to Eur. Phys. J.*
[7] R.D. Heuer, D. Miller, F.Richard and P.M. Zerwas (eds.), et al., *TESLA TDR, Part III: Physics at an* e^+e^- *Linear Collider*, Report DESY-01-011C, http://arXiv.org/abs/hep-ph/0106315.
[8] B. Badelek, et al., *TESLA TDR, Part IV: The Photon Collider at TESLA*, http://arXiv.org/abs/hep-ex/0108012.
[9] I. F. Ginzburg, G. L. Kotkin, V. G. Serbo and V. I. Telnov, Nucl. Instrum. Meth. **205**, 47 (1983).
[10] I. F. Ginzburg, G. L. Kotkin, S. L. Panfil, V. G. Serbo and V. I. Telnov, Nucl. Instrum. Meth. A **219**, 5 (1984).
[11] T. Sjostrand, . T. Sjostrand, P. Eden, C. Friberg, L. Lonnblad, G. Miu, S. Mrenna and E. Norrbin, . See the PYTHIA and JETSET web pages, http://www.thep.lu.se/~torbjorn/Pythia.html.
[12] R. Brun and F. Rademakers, Nucl. Instrum. Meth. A **389**, 81 (1997).
[13] The Pandora web page is http://www-sldnt.slac.stanford.edu/nld/new/Docs/Generators/PANDORA.htm.
[14] P. Chen, G. Horton-Smith, T. Ohgaki, A. W. Weidemann and K. Yokoya, *Nucl. Instrum. Meth.* **A355**, 107 (1995); See http://www-acc-theory.kek.jp/members/cain/cain21b.manual/main.html.
[15] T.Ohgaki,Feb.8,2000, http://arXiv.org/abs/hep-ph/0002083.
[16] S. Heinemeyer, W. Hollik and G. Weiglein, *Phys. Rev.* **D58** (1998) 091701; *Phys. Lett.* **B440** (1998) 296; *Eur. Phys. Jour.* **C16** (2000) 139.
[17] A. Djouadi, J. Kalinowski and M. Spira, *Comput. Phys. Commun.* **108** (1998) 56.
[18] D. Asner, J. Gronberg, J. F. Gunion and T. Hill, Preprint UCRL-ID-143967 (to be submitted to Physical Review D).
[19] G. Jikia and A. Tkabladze, *Phys.Lett.* **B323** (1994) 453-458.
[20] M. Carena, H. E. Haber, H. E. Logan and S. Mrenna, http://arXiv.org/abs/hep-ph/0106116.
[21] H. E. Haber and Y. Nir, Nucl. Phys. B **335**, 363 (1990); H. E. Haber, in *Physics From the Planck Scale to the Electroweak Scale*, Proceedings of the US–Polish Workshop, Warsaw, Poland, September 21–24, 1994, edited by P. Nath, T. Taylor, and S. Pokorski (World Scientific, Singapore, 1995) pp. 49–63 [hep-ph/9501320]; H. E. Haber, M. J. Herrero, H. E. Logan, S. Peñaranda, S. Rigolin and D. Temes, Phys. Rev. D **63**, 055004 (2001).
[22] L. J. Hall, R. Rattazzi and U. Sarid, Phys. Rev. D **50**, 7048 (1994); R. Hempfling, Phys. Rev. D **49**, 6168 (1994); D. M. Pierce, J. A. Bagger, K. T. Matchev and R. Zhang, Nucl. Phys. B **491**, 3 (1997).
[23] M. Carena, M. Olechowski, S. Pokorski and C. E. M. Wagner, Nucl. Phys. B **426**, 269 (1994).
[24] D. Zeppenfeld, R. Kinnunen, A. Nikitenko and E. Richter-Was, Phys. Rev. D **62**, 013009 (2000).
[25] J. F. Gunion and J. G. Kelly, Phys. Lett. **B333**, 110 (1994).
[26] E. Asakawa, S. Y. Choi, K. Hagiwara and J. S. Lee, Phys. Rev. **D62**, 115005 (2000).
[27] P. F. Derwent et al., *Linear Collider Physics*, report prepared for the Fermilab Directorate, http://arXiv.org/abs/hep-ex/0107044.
[28] J. F. Gunion and H. E. Haber, Phys. Rev. D **48**, 5109 (1993).
[29] B. Grzadkowski, J. F. Gunion and J. Kalinowski, Phys. Lett. B **480**, 287 (2000) .
[30] The results of Figure 9 were provided by F. Gianotti on behalf of the ATLAS collaboration. They are the preliminary results available as of March 3, 2001.
[31] G. B. Gelmini and M. Roncadelli, Phys. Lett. B **99**, 411 (1981).
[32] S. Godfrey, P. Kalyniak and N. Romanenko, http://arXiv.org/abs/hep-ph/0108258.

[33] I.F. Ginzburg, et al., Nucl. Instrum. Methods **205**, 47 (1983); *ibid* **219**, 5 (1984); V.I. Telnov, Nucl. Instrum. Methods A **294**, 72 (1990); C. Akerlof, Report No. UM-HE-81-59 (1981; unpublished).
[34] M.L. Swartz, Phys. Rev. D **40**, 1521 (1989); K. Huitu and J. Maalampi, Phys. Lett. B **344**, 217 (1995); H. Fujii, Y. Mimura, K. Sasaki, and T. Sasaki, Phys. Rev. D **49**, 559 (1994); D. Chang and W.-Y. Keung, Phys. Rev. Lett. **62**, 2583 (1989).
[35] U. Bellgardt, et al., Nucl. Phys. B **299**,1 (1988); C. Caso *et al.*, Particle Data Group, Eur. Phys. J. C **3**, 1 (1998); M. L. Brooks *et al.*, Phys. Rev. Lett. **83**, 1521 (1999).
[36] L. Willmann, et al., Phys. Rev. Lett. **82**, 49 (1999).
[37] A. Datta and A. Raychaudhuri, Phys. Rev. D **62**, 055002 (2000); J.F. Gunion, C. Loomis, and K.T. Pitts, *Proceedings of the 1996 DPF/DPB Summer Study on New Directions for High Energy Physics - Snowmass 96*, ed. D.G. Cassel, L. Trindele Gennari, and R.H. Siemann, Snowmass, CO, 1996, p. 603 [hep-ph/9610237].